Technical Note: Feasibility of photoacoustic guided hysterectomies with the da Vinci robot

Margaret Allard,[a] Joshua Shubert,[b] Muyinatu A. Lediju Bell[*] [b,c]

[a]Smith College, Department of Physics, Northampton, MA, USA
[b]Johns Hopkins University, Department of Electrical & Computer Engineering, Baltimore, MD, USA
[c]Johns Hopkins University, Department of Biomedical Engineering, Baltimore, MD, USA

ABSTRACT

This technical note provides an overview of our work to explore the combination of photoacoustic imaging with the da Vinci surgical robot, which is often used to perform teleoperated hysterectomies (i.e., surgical removal of the uterus). Hysterectomies are the prevailing solution to treat medical conditions such as uterine cancer, endometriosis, and uterine prolapse. One complication of hysterectomies is accidental injury to the ureters located within millimeters of the uterine arteries that are severed and cauterized to hinder blood flow and enable full uterus removal. By introducing photoacoustic imaging, we aim to visualize the uterine arteries (and potentially the ureter) during this surgery. We developed a specialized light delivery system to surround a da Vinci curved scissor tool and an ultrasound probe was placed externally, representing a transvaginal approach to receive the resulting acoustic signals. Photoacoustic images were acquired while sweeping the tool across a custom 3D uterine vessel model covered in *ex vivo* bovine tissue that was placed between the 3D model and the light delivery system, as well as between the ultrasound probe and the 3D model (to introduce optical and acoustic scattering). Four tool orientations were explored with the scissors in either open or closed configurations. The optimal tool orientation was determined to be closed scissors with no bending of the tool's wrist, based on measurements of signal contrast and background signal-to-noise ratios in the corresponding photoacoustic images. We also introduce a new metric, $d\theta$, to determine when the image will change during a sweep, based on the tool position and orientation (i.e., pose), relative to previous poses. Overall, results indicate that photoacoustic imaging is a promising approach to enable visualization of the uterine arteries and thereby guide hysterectomies (and other gynecological surgeries). In addition, results can be extended to other minimally invasive da Vinci surgeries and laparoscopic instruments with similar tip geometry.

Keywords: da Vinci® robot, minimally invasive surgery, photoacoustic guided surgery, robotic hysterectomies, surgical navigation, ureter, uterine arteries

1. INTRODUCTION

Surgeons face the often insurmountable task of avoiding critical structures, such as nerves, blood vessels, and ureters, in order to complete surgeries without injuries that lead to severe medical complications and patient death. The primary information available to perform injury-free surgeries include experience, endoscopic camera images, pre-operative MRI or CT images, and in some cases, low-quality, intraoperative images. As an example, injury to the ureter (the tube from the kidneys to the bladder) is one of the most undetected complications of hysterectomies (surgery to remove the uterus), due to poor visualization when the ureter is embedded in surrounding tissue.

Approximately 52-82% of iatrogenic injuries to the ureter occur during gynecologic surgery, often caused by blind clamping, clipping, or cauterizing the of the uterine arteries as they overlap the ureter,[1] which are located within a few millimeters of the uterine artery (see Fig. 1). Ideally this injury would be noticed and addressed as soon as it occurs, yet 50-70% of uretal injuries are undetected during surgery,[2] leading to multiple post operative complications, including kidney failure and death. In addition, hysterectomies are trending toward being performed with assistance from the da Vinci® robot, due to the promise of decreased hospital stays,

*E-mail:mledijubell@jhu.edu

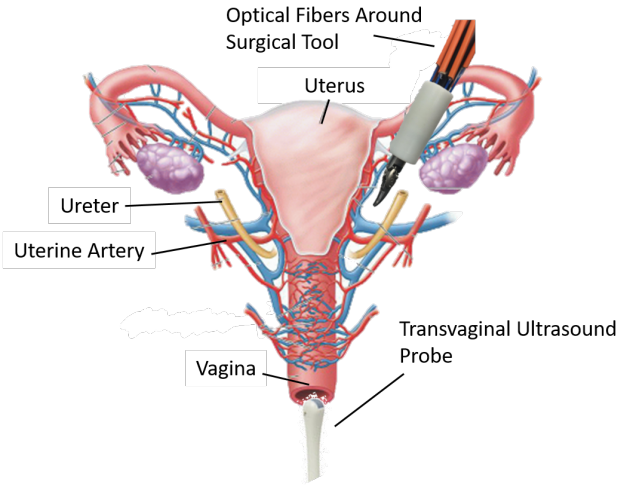

Figure 1: Proposed photoacoustic method for real-time imaging of the ureters and uterine arteries

minimal blood loss, and shorter recovery periods. However, uretal injuries are on the rise with the introduction of robots, as one study documented a 9% increase in the rate of ureter injury during pelvic surgeries performed with robotic technology, when compared to injury rates with no robotic assistance.[3]

The Photoacoustic & Ultrasonic Systems Engineering (PULSE) Lab at Johns Hopkins University is investigating solutions to both detect hidden blood vessels in real time during minimally invasive gynecological surgeries and differentiate these vessels from the ureter using photoacoustic imaging. We are exploring this approach within the context of teleoperated hysterectomies performed with the da Vinci® robot. We envision that optical fibers surrounding a da Vinci® surgical tool would illuminate the surgical site. The uterine arteries, which have higher optical absorption than surrounding tissue, would absorb this light, undergo thermal expansion, and generate a sound wave to be detected with a transvaginal ultrasound probe. Because urine has a low optical absorption,[4–6] our overall vision includes contrast agents for ureter visualization. If a biocompatible contrast agent that is only sensitive to a narrow band of wavelengths[7–9] is inserted into the urinary tract, the ureters can also be visualized with photoacoustic imaging, when the wavelength of the laser is tuned to the optimal wavelength of the contrast agent. With this approach, the surgeon can potentially have more information about the relative positions of the ureter and the uterine arteries. These photoacoustic images can be displayed on the same master console that the surgeon uses for teleoperation.[10,11] In addition, because metal has a high optical absorption coefficient, the da Vinci® tool can also be visualized in the photoacoustic image if it is located within the image plane.

The purpose of this technical note is to summarize the findings of our initial feasibility study published in the *Journal of Medical Imaging, Special Issue on Image-Guided Procedures, Robotic Interventions, and Modeling*.[12] This technical summary is divided into four sections that define the primary contributions and knowledge gained from our initial feasibility testing. Section 2 describes the combined system setup, Section 3 introduces our novel light delivery system design, Section 4 discusses the optimal tool orientation based on contrast measurements and vessel visibility, Section 5 discusses the observed presence of acoustic clutter from the out-of-plane tool tip and its effect on image interpretation for surgical guidance, and Section 6 contains our concluding remarks.

2. COMBINED SYSTEM SETUP

Our experiments were performed in a mock operating room that contained a da Vinci® S robot, consisting of a master console (shown on the right of Fig. 2), patient side manipulators that are teleoperated from the master console (shown on the left of Fig. 2), and an endoscope to visualize the surgical field (shown in the inset of Fig. 2). Only one of the patient side manipulators was used for our experiments, although three of these robot arms are shown in Fig. 2.

A photoacoustic imaging system was positioned next to the mock operating table which contained the experimental phantom (described in more detail below). The photoacoustic imaging system contained an Alpinion

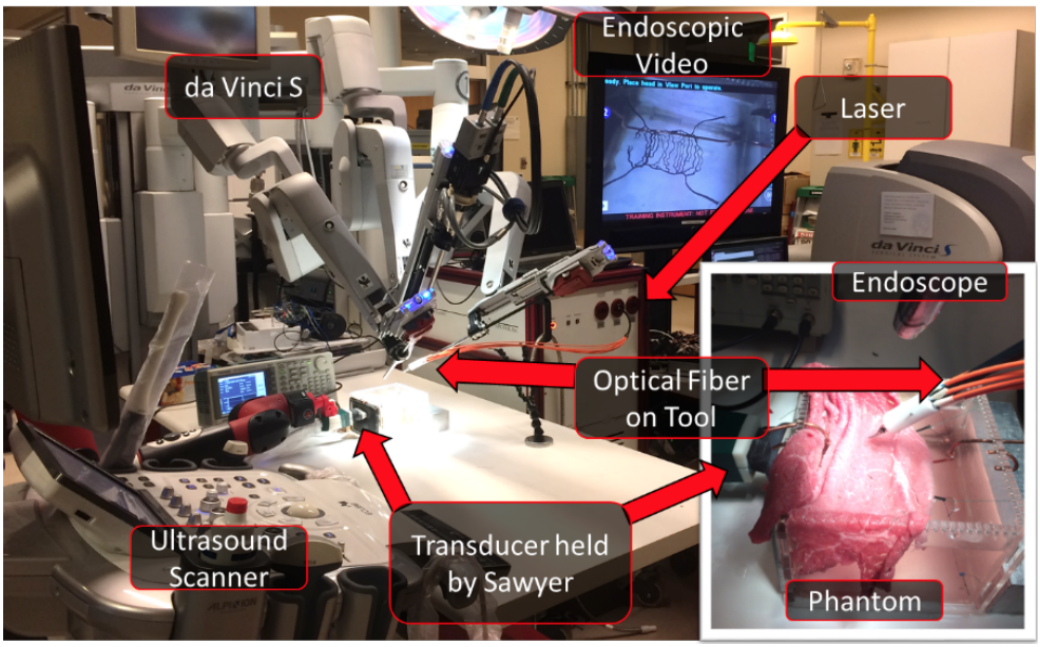

Figure 2: Photograph of the experimental setup. The inset shows a close-up of the phantom used for our experiments, and it demonstrates the relative position of the ultrasound transducer and the optical fibers with respect to the vessel phantom that is covered by *ex vivo* bovine tissue. The uncovered phantom is displayed in the endoscopic video feed.

ECUBE 12R ultrasound system connected to an Alpinion L3-8 linear transducer and a Phocus Mobile laser with a 1-to-7 fiber splitter[13] attached to the 1064-nm output port of the laser. Ideally, the transmitted wavelength would be based on the optimal wavelength required to visualize structures of interest (e.g., 780 nm for deoxygenated hemoglobin). However, because we are imaging a black resin that is expected to have uniform absorption at all wavelengths, we identified 1064 nm to be suitable. The 7 output fibers of the light delivery system surrounded a da Vinci® curved scissor tool, and they were held in place with our custom designed, 3D printed fiber holder (more details in Section 3). The da Vinci® scissor tool was held by one of the patient side manipulators of the da Vinci® S robot.

The custom modular phantom (used in previous work[14]) was built from laser cut acrylic pieces (held in place with silicone glue) and 3D printed components. To simulate the uterine arteries, a 3D model of the arteries around the uterus was designed and 3D printed with black resin. This model was suspended by string through the holes of the phantom, and it is shown in Fig. 2, on the monitor displaying the endoscopic camera video feed.

The phantom was filled with water to permit acoustic wave propagation. The ultrasound transducer was fixed against the acoustic window of the phantom and held by a Sawyer robot (Rethink Robotics), which was used as a stable passive arm for the experiments to ensure that all images were acquired in the same image plane. A 1.5 mm thick layer of *ex vivo* bovine tissue was draped over the phantom (as shown in the inset of Fig. 2), to reside between the optical fiber and the vessels, and another layer of this same tissue was placed inside the phantom, between the 3D model and the transducer. These tissues were placed to introduce both optical and acoustic scattering for photoacoustic imaging.

3. LIGHT DELIVERY SYSTEM DESIGN

We developed a specialized light delivery system to surround a da Vinci® curved scissor tool. A 1-to-7 fiber splitter[13] was attached to the 1064-nm output port of our Opotek Phocus Mobile laser source. The 7 output fibers of the light delivery system surrounded a da Vinci® curved scissor tool, and they were held in place with our custom designed, 3D printed fiber holder, as shown in Fig. 2. Examples of the resulting light profiles are shown in Fig. 3(a).

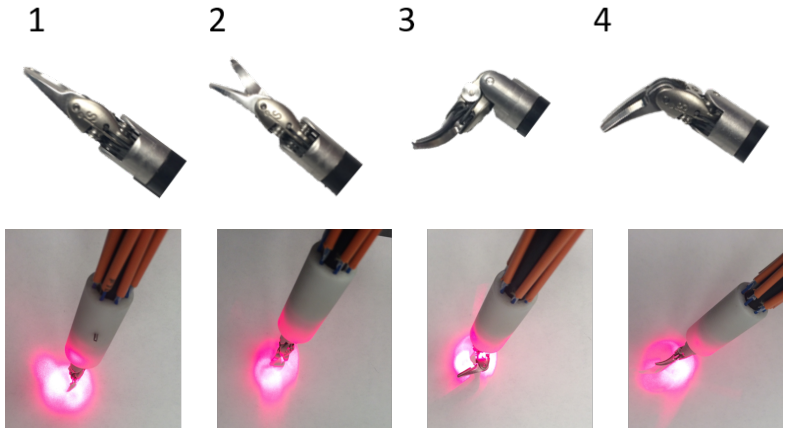

(a)

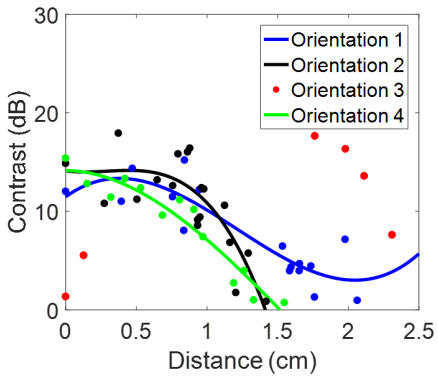

(b)

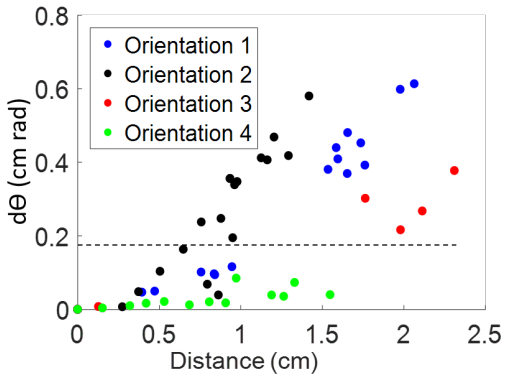

(c)

Figure 3: (a) Photographs of tool Orientations 1 through 4, from left to right, respectively, and corresponding light profiles for tool Orientations 1 through 4, from left to right, respectively, acquired with 635 nm wavelength laser interfaced with the 1-to-7 fiber splitter. (b) Contrast measurements were plotted as a function of distance and fit using third order polynomials. (c) The distance measurements were plotted as a function of our newly defined $d\theta$ metric. A dashed horizontal line was added to show the separation between images acquired when the optical field of view covered the same region of the 3D model as that of the initial starting point for each image. This demarcation was visually determined for each photoacoustic image.

4. OPTIMAL TOOL ORIENTATION

Each da Vinci tool has a wrist for manipulation that is similar to the surgeon's dexterity. As a result, the wrist of the tool can be placed in multiple orientations, with four examples from the same curved scissor tool shown in Fig. 3(a). Orientation 3 blocks more light than Orientation 1, which indicates that part of the underlying structure of interest may have reduced visibility with Orientation 3. Initially, it seemed likely that the optimal tool orientation was tied to the percentage of light that was blocked, which could be related to the percentage of a structure visible in the photoacoustic image, indicating that Orientation 1 is the most optimal orientation. However, we found that the optimal orientation of these four orientations, was not tied to the percentage of light visible. Instead, Orientation 1 was identified as most desirable because it produced the least acoustic clutter (described in more detail in Section 5).

Orientation 3 inspired the introduction of a new metric, $d\theta$, based on both distance from the target and relative orientation based on contrast measurements that did not follow the same trends as distance from the starting point increased, as shown in Fig. 3(b). This metric incorporates the effect of both distance and angular orientation when evaluating changes in image contrast, as shown in Fig. 3(c). This metric can be used to

determine the likelihood that a surgeon will visualize the same structure while sweeping the tool. Generally, based on the results in Fig. 3(c), surgeons will visualize the same region of a photoacoustic target when $d\theta < 0.2$.

5. ACOUSTIC CLUTTER FROM AN OUT-OF-PLANE TOOL TIP

When light from the optical fiber is absorbed by the metal tip of the tool and this tool tip is outside of the image plane, the presence of acoustic clutter from the tool tip could complicate image interpretation. As each tool orientation absorbs varying degrees of light (based on the light profile images in Fig. 3(a)), tool orientation could impact the amount of image clutter present in an image, particularly if the tool tip is outside of the image plane. Example photoacoustic images are shown in Fig. 4(b). Images acquired with Orientation 1 had the least clutter and highest mean background SNR of 1.9. Orientation 2 produced images with slightly more clutter and a mean background SNR of 1.8, while Orientations 3 and 4 produced images with more clutter and mean background SNRs below 1.6. A lower background SNR indicates more clutter, and these background SNR trends are consistent with our interpretation of the source of the acoustic clutter (i.e., absorption of light by the tool tip, which generates out-of-plane acoustic signals).

Acoustic clutter from out-of-plane tools could potentially be mistaken for the tool itself, causing confusion about the true tool location. Results indicate that images acquired with the tool in Orientation 1 produced the least clutter, while images acquired with the tool in Orientation 2 produced slightly more clutter. Orientations 3 and 4 produced images with the most acoustic clutter from the out-of-plane tool tip. This clutter could potentially be mitigated with advanced signal processing methods, including some recent advances in deep learning applied to photoacoustic beamforming.[15–17] In addition, knowledge that the clutter appears deeper in the image could be used to ignore these clutter signals. However, these signals could also be mistaken for the tool residing in the image plane if they are not cleared from the image with advanced signal processing methods.

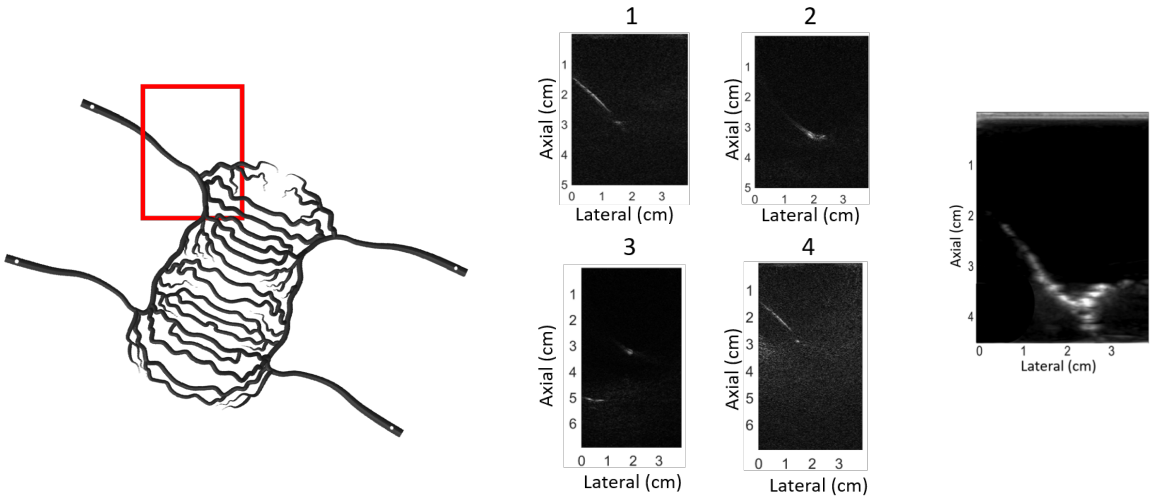

(a) (b) (c)

Figure 4: (a) 3D solid model of vessel structure with red box highlighting the photoacoustic image plane. (b) Photoacoustic image of uterine artery vessel model, acquired with tool Orientations 1-4, as indicated above each image. Orientations 3 and 4 show acoustic clutter below the vessel, which is caused by the out-of-plane tool tip, and the images corresponding to these orientations were extended deeper in order to fully quantify and characterize the contributions from acoustic clutter. (c) Ultrasound image of the vessel phantom, acquired with the ultrasound probe in the same position as that used to acquire the corresponding photoacoustic images. This ultrasound image was acquired prior to the placement of tissue between the transducer and phantom in order to obtain a ground truth image for vessel visibility with minimal acoustic scattering.

6. CONCLUSION

We demonstrated the feasibility of integrating photoacoustic imaging with the da Vinci robot in order to improve targeting of the uterine arteries during hysterectomies. Our integration included a specialized light delivery system to surround a da Vinci curved scissor tool. We additionally provided an analysis of the optimal tool orientations for photoacoustic-guided surgeries using a scissor tool that partially blocks the transmitted light, indicating that the four orientations investigated have the potential to produce sufficient images for photoacoustic guidance. The optimal orientation involved no bending of both the tool's wrist and the joint connecting the scissors. Thus, if a surgeon desires a clear photoacoustic image of the uterine artery or ureter with minimal confusion about the tool location, the best option is to straighten the tool's wrist and close and straighten the scissors if possible. However, to avoid losing sight of a low-contrast signal, it is helpful to lock all angular degrees of freedom before approaching this signal of interest to improve its contrast (instead of adjusting the wrist to achieve the optimal tool orientation). Although the focus of this work is improving hysterectomies performed with a curved scissor tool attached to a da Vinci® robot, our findings are applicable to other da Vinci® tools, other types of da Vinci® surgeries, and laparoscopic surgeries in general that may utilize instruments with similar tip geometry.

Acknowledgements

This work was completed in partnership with the NSF Computational Sensing and Medical Robotics Research Experience for Undergraduates program. Funding was provided by NSF Grant EEC-1460674 and NIH Grant R00-EB018994. The authors thank Anton Deguet, Michelle Graham, Derek Allman, and Formlabs Inc. (Somerville, MA) for their assistance. We additionally acknowledge support from the JHU Carnegie Center for Surgical Innovation.

REFERENCES

1. L. H. Bannister and P. L. Williams, *Gray's anatomy: the anatomical basis of medicine and surgery*, Churchill Livingstone, 1995.
2. S. E. Delacroix and J. Winters, "Urinary tract injures: recognition and management," *Clinics in colon and rectal surgery* **23**(02), pp. 104–112, 2010.
3. S. Rahimi, P. C. Jeppson, L. Gattoc, L. Westermann, S. Cichowski, C. Raker, E. W. LeBrun, and V. Sung, "Comparison of perioperative complications by route of hysterectomy performed for benign conditions," *Female Pelvic medicine & Reconstructive Surgery* **22**(5), pp. 364–368, 2016.
4. S. Feng, W. Chen, Y. Li, G. Chen, Z. Huang, X. Liao, Z. Xie, and R. Chen, "Surface-enhanced raman spectroscopy of urine by an ingenious near-infrared raman spectrometer," in *Photonics Asia 2007*, pp. 682628–682628, 2007.
5. M.-C. Huang, H.-W. Sun, *et al.*, "Study of normal and cancerous urine using photoacoustic spectroscopy," *Journal of Biomedical Engineering* **12**(5), pp. 425–428, 1990.
6. S. Guminetsky, O. V. Pishak, V. P. Pishak, and P. Grigorishin, "Absorbing and diffusive properties of blood plasma and urine proteins," in *International Conference on Correlation Optics*, **3317**, pp. 390–398, 1997.
7. A. Abuteen, S. Zanganeh, J. Akhigbe, L. P. Samankumara, A. Aguirre, N. Biswal, M. Braune, A. Vollertsen, B. Röder, C. Brückner, *et al.*, "The evaluation of nir-absorbing porphyrin derivatives as contrast agents in photoacoustic imaging," *Physical Chemistry Chemical Physics* **15**(42), pp. 18502–18509, 2013.
8. J. Koo, M. Jeon, Y. Oh, H. W. Kang, J. Kim, C. Kim, and J. Oh, "In vivo non-ionizing photoacoustic mapping of sentinel lymph nodes and bladders with icg-enhanced carbon nanotubes," *Physics in Medicine and Biology* **57**(23), p. 7853, 2012.
9. C. L. Bayer, J. Kelvekar, and S. Y. Emelianov, "Influence of nanosecond pulsed laser irradiance on the viability of nanoparticle-loaded cells: implications for safety of contrast-enhanced photoacoustic imaging," *Nanotechnology* **24**(46), p. 465101, 2013.
10. S. Kim, Y. Tan, P. Kazanzides, and M. A. Lediju Bell, "Feasibility of photoacoustic image guidance for telerobotic endonasal transsphenoidal surgery," in *IEEE International Conference on Biomedical Robotics and Biomechatronics*, 2016.

11. S. Kim, N. Gandhi, M. A. L. Bell, and P. Kazanzides, "Improving the safety of telerobotic drilling of the skull base via photoacoustic sensing of the carotid arteries," in *Robotics and Automation (ICRA), 2017 IEEE International Conference on*, pp. 2385–2390, IEEE, 2017.
12. M. Allard, J. Shubert, and M. A. L. Bell, "Feasibility of photoacoustic guided teleoperated hysterectomies," *Journal of Medical Imaging: Special Issue on Image-Guided Procedures, Robotic Interventions, and Modeling* **5**(2), p. 021213, 2018.
13. B. Eddins and M. A. L. Bell, "Design of a multifiber light delivery system for photoacoustic-guided surgery," *Journal of Biomedical Optics* **22**(4), 2017.
14. N. Gandhi, M. Allard, S. Kim, P. Kazanzides, and M. Lediju Bell, "Photoacoustic-based approach to surgical guidance performed with and without a da vinci robot," *Journal of Biomedical Optics* **22**(12), p. 121606, 2017.
15. A. Reiter and M. A. L. Bell, "A machine learning approach to identifying point source locations in photoacoustic data," in *Proc. of SPIE Vol*, **10064**, pp. 100643J–1, 2017.
16. D. Allman, A. Reiter, and M. A. L. Bell, "A machine learning method to identify and remove reflection artifacts in photoacoustic channel data," in *IEEE International Ultrasonics Symposium*, 2017.
17. D. Allman, A. Reiter, and M. A. L. Bell, "Exploring the effects of transducer models when training convolutional neural networks to eliminate reflection artifacts in experimental photoacoustic images," in *Proc. of SPIE Vol*, **10494**, 2018.